Modeling of the perfect electromagnetic conducting boundary in the finite difference time domain method

Vahid Nayyeri,[1,2] Mohammad Soleimani,[2] and Mojtaba Dehmollaian[3]

Received 10 February 2013; revised 11 June 2013; accepted 21 July 2013.

[1] The perfect electromagnetic conducting (PEMC) boundary, a nonreciprocal generalization of both perfect electric conducting (PEC) and perfect magnetic conducting (PMC) boundaries, is modeled in the finite difference time domain (FDTD) method. Since the PEMC boundary condition requires collocation of same components of both electric and magnetic fields at the boundary grids, which is not compatible with the original FDTD algorithm, its implementation in FDTD is challenging and requires modification in the algorithm. To do this task, first, the original FDTD cell is modified by inserting the required field components not present in the original cell. Then, a novel formulation is developed for updating fields' components at the boundary. Modeling of a PEMC planar interface, a corner point, and a wedge point are presented. Finally, numerical examples are presented to show stability, accuracy, and applicability of the proposed approach. Validation is achieved by comparisons with existing analytic methods and/or conventional FDTD for special cases of PEC and PMC boundaries.

Citation: Nayyeri, V., M. Soleimani, and M. Dehmollaian (2013), Modeling of the perfect electromagnetic conducting boundary in the finite difference time domain method, *Radio Sci.*, *48*, doi:10.1002/rds.20051.

1. Introduction

[2] A perfect electromagnetic conductor (PEMC) is a nonreciprocal generalization of both a perfect electric conductor (PEC) and a perfect magnetic conductor (PMC), which was introduced by *Lindell and Sihvola* [2005a]. It is shown that fields cannot convey energy into a PEMC medium; hence, the PEMC is considered as an ideal boundary given by the following condition [*Lindell and Sihvola*, 2006a, 2009]:

$$\hat{\boldsymbol{n}} \times (\boldsymbol{H} + M\boldsymbol{E}) = 0, \text{i.e.,} \boldsymbol{H}_t = -M\boldsymbol{E}_t, \tag{1}$$

where M is a scalar real parameter denoting the PEMC admittance, $\hat{n}$ denotes the unit vector normal to the boundary, and subscript t stands for tangential components of the fields (i.e., electric $\boldsymbol{E}$ and magnetic $\boldsymbol{H}$). Obviously, for $M \to \pm\infty$ and $M = 0$, the boundary condition (1) reduces to $\hat{n} \times \boldsymbol{E} = 0$ and $\hat{n} \times \boldsymbol{H} = 0$, corresponding to PEC and PMC boundaries, respectively. The PEMC boundary can be also considered as a special type of surface impedance boundary. The general form of surface impedance boundary condition (SIBC), which is a linear relation between time-harmonic electric and magnetic field components tangential to the boundary surface, can be written as [*Wallen et al*., 2011]

$$\boldsymbol{E}_t = \overline{\overline{\boldsymbol{Z}}}_s \cdot \hat{\boldsymbol{n}} \times \boldsymbol{H}, \tag{2}$$

where $\overline{\overline{Z}}_s$ is the two-dimensional (2-D) surface impedance dyadic. For an isotropic impedance boundary (regular impedance boundary), $\overline{\overline{Z}}_s = Z_s \overline{\overline{I}}$, while for the PEMC boundary condition (1)

$$\overline{\overline{\boldsymbol{Z}}}_s = \frac{1}{M} \hat{\boldsymbol{n}} \times \overline{\overline{\boldsymbol{I}}},$$

where $\overline{\overline{\mathrm{I}}}$ is the two-dimensional (2-D) identity dyadic. Equation (2) clearly shows creation of nonreciprocal reflection, which is the most motivating property of the PEMC boundary. Due to this property, the PEMC boundary has many rich potential applications in electromagnetics, particularly for polarization transforming purposes [*Lindell and Sihvola*, 2005b, 2006b; *Sihvola and Lindell*, 2006; *Nayyeri et al*., 2012a, 2012b]. Hence, some approaches were introduced for the realization of the PEMC boundary [*Lindell and Sihvola*, 2005c, 2006c]. Recently, it has been practically realized by a grounded ferrite slab (as shown in Figure 1), where the effect of Faraday rotation, supported by a magnetically biased ferrite, was used [*Shahvarpour et al*., 2010].

[3] The electromagnetic wave interaction with the PEMC boundary is investigated in many studies such as *Lindell and Sihvola* [2005b], *Ruppin* [2006], *Komijani and Rashed-Mohassel* [2009a], *Rasouli Disfani et al*. [2011], and *Nayyeri et al*. [2012a]; however, due to the complexity of the boundary, analytic solutions are available only for relatively simple problems. On the other hand, numerical evaluation of such problems was considered only in *Sihvola et al*. [2007], where scattering by a small PEMC sphere was addressed. Thus,

[1]Department of Electrical and Computer Engineering, University of Waterloo, Waterloo, Ontario, Canada.
[2]School of Electrical Engineering, Iran University of Science and Technology, Tehran, Iran.
[3]Center of Excellence on Applied Electromagnetic Systems, School of Electrical and Computer Engineering, University of Tehran, Tehran, Iran.

Corresponding author: V. Nayyeri, Department of Electrical and Computer Engineering, University of Waterloo, Waterloo, ON N2L3G1, Canada. (nayyeri@ieee.org)

0048-6604/13/10.1002/rds.20051

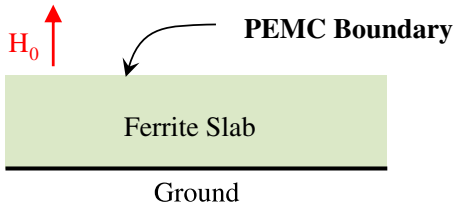

Figure 1. Practical realization of a PEMC boundary by a grounded ferrite slab as proposed by *Shahvarpour et al.* [2010].

implementation of the PEMC boundary using numerical techniques that can treat an arbitrary problem is valuable.

[4] The finite difference time domain (FDTD) method [*Yee*, 1966; *Taflove and Hagness*, 2005; *Elsherbeni and Demir*, 2009; *Sullivan*, 2000; *Kunz and Luebbers*, 1993] is one of the most powerful computational electromagnetics methods, particularly for solving electromagnetic wave interaction with complex media and boundaries [*Young*, 1994; *Schuster and Luebbers*, 1996; *Teixeira*, 2008; *Nayyeri et al.*, 2011a; *Nayyeri et al.*, 2013]. The FDTD method is based on decomposition, discretization, and simultaneous solution of the Maxwell curl equations in the time and space domains using updating equations for $\boldsymbol{E}$ and $\boldsymbol{H}$. In problems involving boundary conditions like PEC, PMC, SIBC, etc., an updating equation for $\boldsymbol{E}$ or $\boldsymbol{H}$ at the boundary is required. For instance, at a PEC boundary, values of tangential $\boldsymbol{E}$ are set to zero at all time steps. On the other hand, for a PEMC, the boundary condition (1) or (2) is a nonreciprocal mixed one, involving both $\boldsymbol{E}$ and $\boldsymbol{H}$. Thus, the most challenging part in FDTD implementation is the fact that *same components* of both $\boldsymbol{E}_t$ and $\boldsymbol{H}_t$ need to be colocated at both time and space, not realizable with the algorithm of *Yee* [1966]. Of course, this is unlike the implementation of the (regular) SIBC (first proposed by *Maloney and Smith* [1992] and *Beggs et al.* [1992]), where $\boldsymbol{E}_t = Z_s[\hat{n}\times\boldsymbol{H}_t]$ and the *cross components* of $\boldsymbol{E}_t$ and $\boldsymbol{H}_t$ need to be colocated, more easily realizable with Yee's algorithm. In the latter (implementation of SIBC), $\boldsymbol{H}_t$ at the interface is commonly approximated by its value at a half a cell size in front of the interface. Previously, in a conference paper [*Nayyeri et al.*, 2011b], which addressed plane wave reflection from a PEMC planar interface, we used the same approximation for implanting a PEMC planar interface in the one-dimensional (1-D) FDTD method. However, this technique could not be applied for modeling of the PEMC boundary in the 2-D and 3-D FDTD algorithms. For clarity, using this approximation couples updating equations for all the boundary grids to each other, which is, of course, not applicable.

[5] Basically, in the present paper, we propose an approach for modeling of an arbitrary PEMC boundary in the FDTD method. The PEMC boundary condition (1) is implemented in the FDTD method by a new formulation based on modifying the original Yee cell and using the backward difference scheme (BDS)/forward difference scheme (FDS) for the approximation of the field components at the boundary. The abstract of using the BDS for this purpose is briefly presented by the authors in *Nayyeri et al.* [2012c]. The proposed formulation is applied for modeling of PEMC planar interface, corner, and wedge. Full validation of the method is also presented.

2. Implementation of the PEMC Boundary Condition in the FDTD Method

[6] In this section, derivation of fields updating equations at a PEMC boundary with a planar interface, a corner point, and a wedge point is presented. To do this task, first, the traditional Yee cell is modified, and second, the decomposed Maxwell curl equations are properly discretized. The central difference scheme (CDS) is used for spatial derivatives along the boundary, and the BDS/FDS is used for the spatial derivatives normal to the boundary. To ensure the stability of the method, the time derivatives are carried out using the CDS. Third, the PEMC boundary condition (1) is applied on the discretized equations. Basically, the value of some required field components not observed in the modified cell grid is approximated by averaging values of the components at the adjacent grids. The implementation of the PEMC boundary condition in 1-D and 2-D FDTD algorithms is presented in the following. Here we note that the proposed algorithm can be extended to a 3-D method as well.

2.1. Implementation in 1-D FDTD

[7] Let us consider a planar free-space PEMC interface, as shown in Figure 2, where a 1-D FDTD grid based on Yee's algorithm and locations of $\boldsymbol{E}$ and $\boldsymbol{H}$ at neighboring grids are demonstrated. Since a PEMC interface rotates the polarization of incident wave (i.e., the reflection from the interface due to a normal incidence of a plane wave has both co- and cross-polarized components), both the x and y components of $\boldsymbol{E}$ and $\boldsymbol{H}$ are considered in computations. We are interested to derive updating equations for the field components at the boundary. To do this, let us start with Amper's law, $\nabla\times\boldsymbol{H}=\partial\boldsymbol{D}/\partial t$. By first decomposing and next discretizing the equation, at the grid $K+1$, we obtain

$$\frac{\varepsilon_0}{\Delta t}\left[E_x^{n+1}(K+1)-E_x^{n}(K+1)\right] = -\frac{2}{\delta}\left[H_y^{n+1/2}(K+1)-H_y^{n+1/2}(K+1/2)\right], \tag{3a}$$

$$\frac{\varepsilon_0}{\Delta t}\left[E_y^{n+1}(K+1)-E_y^{n}(K+1)\right] = \frac{2}{\delta}\left[H_x^{n+1/2}(K+1)-H_x^{n+1/2}(K+1/2)\right], \tag{3b}$$

where Δt and δ, respectively, are the time and space steps. Here it is noted that the CDS and the BDS, respectively, are used for the time and spatial derivatives along normal to the interface, i.e., the z direction. Since the PEMC interface

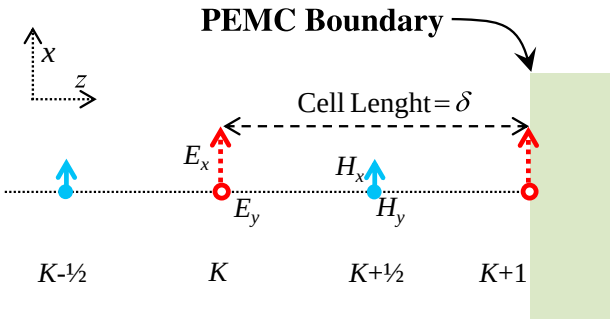

Figure 2. A 1-D FDTD mesh and a planar PEMC interface at grid $K+1$.

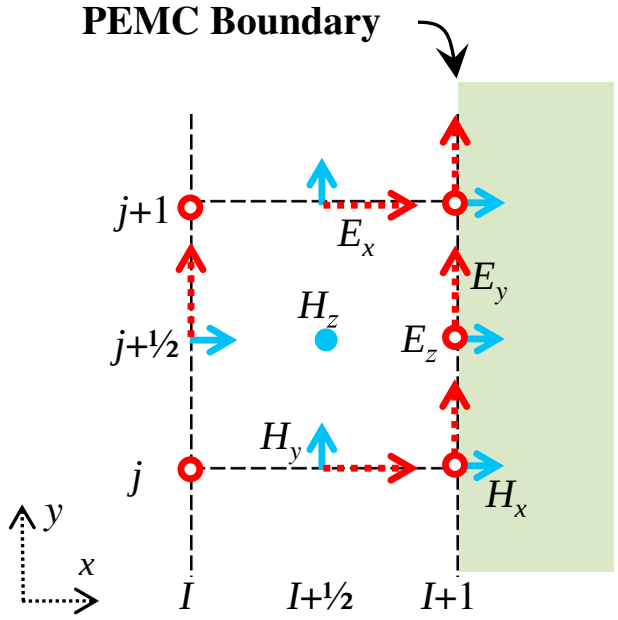

Figure 3. Modified 2-D FDTD mesh, including a PEMC boundary. Components of magnetic and electric fields are denoted by solid and dashed arrows, respectively.

isat grid $K+1$, fields at this grid follow the boundary condition (1) as

$$H_x(K+1) = -ME_x(K+1), \tag{4a}$$

$$H_y(K+1) = -ME_y(K+1). \tag{4b}$$

[8] Now, first, by substituting equations (4a) and (4b) in equations (3a) and (3b); second, by approximating the $\boldsymbol{E}$ components at time step $n+½$ by the average of those estimated at a half a time step in the future and the past, i.e., ${E_{x,y}}^{n+½} \approx ½({E_{x,y}}^{n+1} + {E_{x,y}}^{n})$; and, third, by collecting the $\boldsymbol{E}$ components at time step $n+1$ in the left-hand sides of equations (3a) and (3b), the following system of equations is obtained:

$$\begin{bmatrix} 1 & -MC_e \\ MC_e & 1 \end{bmatrix} \begin{bmatrix} E_x^{n+1}(K+1) \\ E_y^{n+1}(K+1) \end{bmatrix} = \begin{bmatrix} R_1 \\ R_2 \end{bmatrix}, \tag{5}$$

where $C_e = \Delta t/\varepsilon_0\delta$, and R_1 and R_2 are functions of $\boldsymbol{E}$ and $\boldsymbol{H}$ components at time steps n and $n+½$ defined by

$$R_1 = E_x^n(K+1) + MC_eE_y^n(K+1) + 2C_eH_y^{n+½}(K+½),$$

$$R_2 = -MC_eE_x^n(K+1) + E_y^n(K+1) - 2C_eH_x^{n+½}(K+½).$$

[9] Solving the above system of two linear equations for ${E_x}^{n+1}(K+1)$ and ${E_y}^{n+1}(K+1)$, we obtain updating equations for the x and y components of $\boldsymbol{E}$ at the PEMC interface as

$$E_x^{n+1}(K+1) = \frac{1}{1+M^2C_e^2}(R_1 + MC_eR_2), \tag{6a}$$

$$E_y^{n+1}(K+1) = \frac{1}{1+M^2C_e^2}(-MC_eR_1 + R_2), \tag{6b}$$

where $1+M^2{C_e}^2$ is the determinant of the coefficients in equation (5). Since the determinant is always (for any real value of M) nonzero, the result is valid for all values of M.

[10] Basically, using equations (6a) and (6b), the electric field components at the PEMC interface $[{E_{x,y}}^{n+1}(K+1)]$ are updated by the following: (1) their values at a time step in the past $[{E_{x,y}}^{n}(K+1)]$ and (2) values of the $\boldsymbol{H}$ components at a half a cell size in front of the interface and at a half a time step in the past $[{H_{x,y}}^{n+½}(K+½)]$. This way, the PEMC boundary condition in a 1-D FDTD technique is implemented.

2.2. Implementation in 2-D FDTD

[11] Usually, classic 2-D problems are decomposed into two separate problems, namely, transverse electric (TE) and transverse magnetic (TM) cases, each including separate three field components; a 2-D FDTD technique may consider one of the TE or TM cases. On the other hand, in problems involving PEMC, since the incident field experiences rotation upon reflection from the PEMC boundary, all $\boldsymbol{E}$ and $\boldsymbol{H}$ components need to be considered in the FDTD computations. Furthermore, the PEMC boundary condition (1) requires the same components of $\boldsymbol{E}$ and $\boldsymbol{H}$ to be colocated in space (and time), while those are not colocated in a conventional Yee's algorithm. Hence, the original Yee cell needs to be modified. The modified FDTD cell is shown in Figure 3, for which no variation along the z direction is assumed and a PEMC boundary is placed at nodes indexed by $i = I+1$. Comparing the FDTD cell shown in Figure 3 with the original FDTD cell, the following modifications are applied.

[12] 1. Both TE and TM field components are considered in grids (i.e., the TE and TM cells are overlapped).

[13] 2. Both tangential (z and y) components of $\boldsymbol{E}$ and the normal (x) component of $\boldsymbol{H}$ at each node on the PEMC boundary are included in computations.

[14] Accordingly, the field components at the PEMC boundary are categorized into two groups: (1) the main field components included in an original FDTD cell, including both TE_z and TM_z field components, E_z at node $(I+1, j)$, and E_y and H_x at node $(I+1, j+½)$; and (2) auxiliary field components, not included in an original FDTD cell, E_z at node $(I+1, j+½)$, and E_y and H_x at node $(I+1, j)$.

[15] Having these modifications, fields updating equations at the boundary are given by the following five steps.

[16] First, Amper's law, $\nabla \times \boldsymbol{H} = \partial \boldsymbol{D}/\partial t$ is properly discretized at grid $(I+1, j+½)$. That is, the CDS is used for time derivatives and spatial derivatives along the y direction (parallel to the boundary), and the BDS is used for spatial derivatives along the x direction (normal to the boundary). Assuming δ_x and δ_y, respectively, are steps along x and y directions, we have

$$E_y^{n+1}(I+1, j+{}^1\!/_2) = E_y^n(I+1, j+{}^1\!/_2) - \frac{2\Delta t}{\varepsilon_0\delta_x}\left[H_z^{n+1/2}(I+1, j+{}^1\!/_2) - H_z^{n+1/2}\left(I+{}^1\!/_2, j+{}^1\!/_2\right)\right],$$

$$E_z^{n+1}(I+1, j+{}^1\!/_2) = E_z^n(I+1, j+{}^1\!/_2) + \frac{2\Delta t}{\varepsilon_0\delta_x}[H_y^{n+1/2}(I+1, j+{}^1\!/_2) - H_y^{n+1/2}(I+{}^1\!/_2, j+{}^1\!/_2)) - \frac{\Delta t}{\varepsilon_0\delta_y}[H_x^{n+1/2}(I+1, j+1) - H_x^{n+1/2}(I+1, j)).$$

[17] Second, by substituting the PEMC boundary condition (1) at grid $(I+1, j+½)$, given by $H_{y,z}(I+1, j+½) = -ME_{y,z}(I+1, j+½)$ in the above equations, we obtain

$$E_y^{n+1}(I+1,j+\tfrac{1}{2}) = E_y^n(I+1,j+\tfrac{1}{2}) - \frac{2\Delta t}{\varepsilon_0\delta_x}\left[-M E_z^{n+\frac{1}{2}}(I+1,j+\tfrac{1}{2}) - H_z^{n+\frac{1}{2}}(I+\tfrac{1}{2},j+\tfrac{1}{2})\right], \quad (7a)$$

$$E_z^{n+1}(I+1,j+\tfrac{1}{2}) = E_z^n(I+1,j+\tfrac{1}{2}) - \frac{2\Delta t}{\varepsilon_0\delta_x}\left[M E_y^{n+\frac{1}{2}}(I+1,j+\tfrac{1}{2}) + H_y^{n+\frac{1}{2}}(I+\tfrac{1}{2},j+\tfrac{1}{2})\right] - \frac{\Delta t}{\varepsilon_0\delta_y}\left[H_x^{n+\frac{1}{2}}(I+1,j+1) - H_x^{n+\frac{1}{2}}(I+1,j)\right]. \quad (7b)$$

[18] Third, in equation (7b), the y component of $\boldsymbol{H}$ at grid $(I+\frac{1}{2}, j+\frac{1}{2})$ is observed, not defined at the modified 2-D mesh (see Figure 3). Thus, it should be approximated by the average of the same components at neighboring grids $(I+\frac{1}{2}, j+1)$ and $(I+\frac{1}{2}, j)$ [i.e., $H_y(I+\frac{1}{2}, j+\frac{1}{2}) \approx \frac{1}{2}(H_y(I+\frac{1}{2}, j+1)+H_y(I+\frac{1}{2}, j))$]. In addition, since the values of $\boldsymbol{E}$ components are updated at integer time steps, the components of $\boldsymbol{E}$ at $(n+\frac{1}{2})$ should be estimated by the average of values at time steps n and $n+1$ [i.e., ${E_{y,z}}^{n+\frac{1}{2}} \approx \frac{1}{2}({E_{y,z}}^{n+1} + {E_{y,z}}^{n})$]. Afterward, collecting the $\boldsymbol{E}$ components at time step $n+1$ in the left-hand sides, we obtain the following system of equations for tangential components of $\boldsymbol{E}$ at grid $(I+1, j+\frac{1}{2})$:

$$\begin{bmatrix} 1 & -MC_{ex} \\ MC_{ex} & 1 \end{bmatrix} \begin{bmatrix} E_y^{n+1}(I+1,j+\frac{1}{2}) \\ E_z^{n+1}(I+1,j+\frac{1}{2}) \end{bmatrix} = \begin{bmatrix} S_1^{n+\frac{1}{2}} \\ S_2^{n+\frac{1}{2}} \end{bmatrix}, \quad (8)$$

where ${S_1}^{n+\frac{1}{2}}$ and ${S_2}^{n+\frac{1}{2}}$ are functions of $\boldsymbol{E}$ and $\boldsymbol{H}$ components at time steps n and $n+\frac{1}{2}$ defined by

$$S_1^{n+\frac{1}{2}} = E_y^n(I+1,j+\tfrac{1}{2}) + MC_{ex}E_z^n(I+1,j+\tfrac{1}{2}) + 2C_{ex}H_z^{n+\frac{1}{2}}(I+\tfrac{1}{2},j+\tfrac{1}{2}), \quad (9a)$$

$$S_2^{n+\frac{1}{2}} = -MC_{ex}E_y^n(I+1,j+\tfrac{1}{2}) + E_z^n(I+1,j+\tfrac{1}{2}) - C_{ex}\left[H_y^{n+\frac{1}{2}}(I+\tfrac{1}{2},j+1) + H_y^{n+\frac{1}{2}}(I+\tfrac{1}{2},j)\right] - C_{ey}\left[H_x^{n+\frac{1}{2}}(I+1,j+1) - H_x^{n+\frac{1}{2}}(I+1,j)\right], \quad (9b)$$

and $C_{ex} = \Delta t/\varepsilon_0\delta_x$ and $C_{ey} = \Delta t/\varepsilon_0\delta_y$. In a similar way, at grid $(I+1, j)$, we have

$$\begin{bmatrix} 1 & -MC_{ex} \\ MC_{ex} & 1 \end{bmatrix} \begin{bmatrix} E_y^{n+1}(I+1,j) \\ E_z^{n+1}(I+1,j) \end{bmatrix} = \begin{bmatrix} T_1^{n+\frac{1}{2}} \\ T_2^{n+\frac{1}{2}} \end{bmatrix}, \quad (10)$$

where ${T_1}^{n+\frac{1}{2}}$ and ${T_2}^{n+\frac{1}{2}}$ are defined by

$$T_1^{n+\frac{1}{2}} = E_y^n(I+1,j) + MC_{ex}E_z^n(I+1,j) + C_{ex}\left[H_z^{n+\frac{1}{2}}(I+\tfrac{1}{2},j+\tfrac{1}{2}) + H_z^{n+\frac{1}{2}}(I+\tfrac{1}{2},j-\tfrac{1}{2})\right], \quad (11a)$$

$$T_2^{n+\frac{1}{2}} = E_z^n(I+1,j) - MC_{ex}E_y^n(I+1,j) - 2C_{ex}H_y^{n+\frac{1}{2}}(I+\tfrac{1}{2},j) - C_{ey}\left[H_x^{n+\frac{1}{2}}(I+1,j+\tfrac{1}{2}) - H_x^{n+\frac{1}{2}}(I+1,j-\tfrac{1}{2})\right]. \quad (11b)$$

[19] It is noted that in deriving equation (11a), the z component of $\boldsymbol{H}$ at grid $(I+\frac{1}{2}, j)$ is approximated by the average of its values at grids $(I+\frac{1}{2}, j+\frac{1}{2})$ and $(I+\frac{1}{2}, j-\frac{1}{2})$.

[20] Fourth, the updating equations for the tangential components of $\boldsymbol{E}$ at grid $(I+1, j+\frac{1}{2})$ is obtained by solving system of equations (8), given by

$$E_y^{n+1}(I+1,j+\tfrac{1}{2}) = \frac{1}{1+M^2C_{ex}^2}\left(S_1^{n+\frac{1}{2}} + MC_{ex}S_2^{n+\frac{1}{2}}\right), \quad (12a)$$

$$E_z^{n+1}(I+1,j+\tfrac{1}{2}) = \frac{1}{1+M^2C_{ex}^2}\left(S_2^{n+\frac{1}{2}} - MC_{ex}S_1^{n+\frac{1}{2}}\right), \quad (12b)$$

and the updating equations of $\boldsymbol{E}$ components at grid $(I+1, j)$ are achieved by solution of (10) as follows:

$$E_y^{n+1}(I+1,j) = \frac{1}{1+M^2C_{ex}^2}\left(T_1^{n+\frac{1}{2}} + MC_{ex}T_2^{n+\frac{1}{2}}\right), \quad (13a)$$

$$E_z^{n+1}(I+1,j) = \frac{1}{1+M^2C_{ex}^2}\left(T_2^{n+\frac{1}{2}} - MC_{ex}T_1^{n+\frac{1}{2}}\right). \quad (13b)$$

[21] Here it is noted that the determinant of the coefficient matrix in equations (8) and (10) is $1+M^2{C_{ex}}^2$, always nonzero. Therefore, equations (12a), (12b), (13a), and (13b) can be used for any values of M.

[22] Fifth, according to equations (9b) and (11b), the x component (normal component) of $\boldsymbol{H}$ at nodes on the PEMC boundary is needed to update tangential components of $\boldsymbol{E}$. Hence, this component of $\boldsymbol{H}$ (which is included in the modified 2-D mesh (Fig. 3)) is updated at time steps $(n+\frac{1}{2})$. The updating equation is simply derived by discretizing Faraday's law, $\nabla \times \boldsymbol{E} = -\partial \boldsymbol{B}/\partial t$, as

$$H_x^{n+\frac{1}{2}}(I+1,j+\tfrac{1}{2}) = H_x^{n-\frac{1}{2}}(I+1,j+\tfrac{1}{2}) - \frac{\Delta t}{\mu_0\delta_y}\left[E_z^n(I+1,j+1) - E_z^n(I+1,j)\right], \quad (14a)$$

$$H_x^{n+\frac{1}{2}}(I+1,j) = H_x^{n-\frac{1}{2}}(I+1,j) - \frac{\Delta t}{\mu_0\delta_y}\left[E_z^n(I+1,j+\tfrac{1}{2}) - E_z^n(I+1,j-\tfrac{1}{2})\right]. \quad (14b)$$

[23] At this point, all the updating equations for the field components at the PEMC boundary are completed. We can summarize the process in the following order: (1) updating x (normal) component of the magnetic field using equations (14a) and (14b); (2) updating S_1, S_2, T_1, and T_2 using equations (9a), (9b), (11a), and (11b); and (3) updating y and z (tangential) components of the electric field using equations (12a), (12b), (13a), and (13b).

[24] One should note that the main field components [i.e., E_z at node $(I+1, j)$ and E_y and H_x at node $(I+1, j+\frac{1}{2})$] are used not only for updating field components at the boundary but also for updating field components at neighboring grids indexed by $i = I+\frac{1}{2}$. On the other hand, the auxiliary field components [i.e., E_z at node $(I+1, j+\frac{1}{2})$ and E_y and H_x at node $(I+1, j)$] are used only for updating fields at the PEMC boundary.

[25] Now we may apply the presented method to an arbitrary 2-D PEMC object. Of course, the boundary is first modeled by connected wedges and corners. Hence, it is necessary to propose a method for updating fields at the PEMC corner and wedge points. Figures 4a and 4b show a PEMC corner and a wedge, respectively. Modified 2-D FDTD meshes are also illustrated in these figures. First, let us consider the corner case shown in Figure 4a and derive the field updating equations at the node $(I+1, J+1)$. Here we note that fields at the boundary nodes adjacent to the corner,

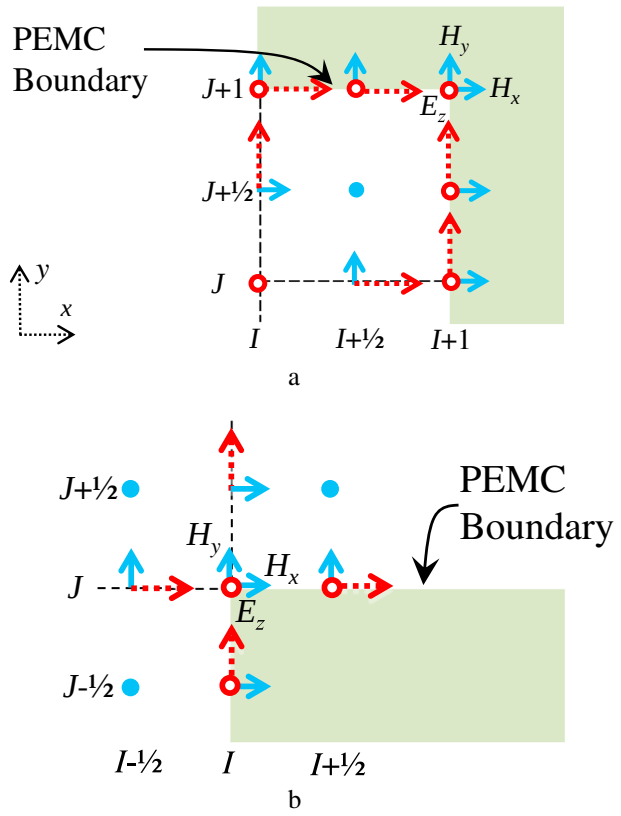

Figure 4. A 2-D FDTD mesh, including (a) a PEMC corner and (b) a wedge. Components of magnetic and electric fields are denoted by solid and dashed arrows, respectively.

i.e., $(I+1, J+½)$ and $(I+½, J+1)$, require the following components of $\boldsymbol{E}$ and $\boldsymbol{H}$ at the corner node $(I+1, J+1)$ to be updated.

[26] 1. ${H_x}^{n+½}(I+1, J+1)$ is required for updating ${E_y}^{n+1}(I+1, J+½)$ and ${E_z}^{n+1}(I+1, J+½)$ [see equations (12a) and (12b)].

[27] 2. ${H_y}^{n+½}(I+1, J+1)$ is required for updating ${E_x}^{n+1}(I+½, J+1)$ and ${E_z}^{n+1}(I+½, J+1)$.

[28] 3. ${E_z}^{n}(I+1, J+1)$ is required for updating ${H_x}^{n+½}(I+1, J+½)$ and ${H_y}^{n+½}(I+½, J+1)$ [see equation (14a)].

[29] Hence, in the modified 2-D mesh, the z component of $\boldsymbol{E}$ and the x and y components of $\boldsymbol{H}$ are required at the node $(I+1, J+1)$. The field updating equations for these components are derived by discretizing Maxwell's curl equation for $\boldsymbol{H}$ as follows:

$$E_x^{n+1}(I+1,J+1) = E_x^n(I+1,J+1) + 2C_{ey}[H_z^{n+½}(I+1,J+1) - H_z^{n+½}(I+1,J+{}^1/_2)],$$

$$E_y^{n+1}(I+1,J+1) = E_y^n(I+1,J+1) - 2C_{ex}[H_z^{n+½}(I+1,J+1) - H_z^{n+½}(I+½,J+1)],$$

$$E_z^{n+1}(I+1,J+1) = E_z^n(I+1,J+1) + 2C_{ex}[H_y^{n+½}(I+1,J+1) - H_y^{n+½}(I+½,J+1)] - 2C_{ey}[H_x^{n+½}(I+1,J+1) - H_x^{n+½}(I+1,J+½)],$$

where coefficients C_{ex} and C_{ey} are defined previously after equations (9a) and (9b). It is noticed that the BDS is used for the spatial derivatives along both the x and y directions. Now by applying the PEMC boundary condition (1), we get

$$E_x^{n+1}(I+1,J+1) = E_x^n(I+1,J+1) - 2C_{ey}M[E_z^{n+½}(I+1,J+1) - E_z^{n+½}(I+1,J+½)],$$

$$E_y^{n+1}(I+1,J+1) = E_y^n(I+1,J+1) + 2C_{ex}M[E_z^{n+½}(I+1,J+1) - E_z^{n+½}(I+½,J+1)],$$

$$E_z^{n+1}(I+1,J+1) = E_z^n(I+1,J+1) - 2C_{ex}[ME_y^{n+½}(I+1,J+1) + H_y^{n+½}(I+1,J+1)] + 2C_{ey}[ME_x^{n+½}(I+1,J+1) + H_x^{n+½}(I+1,J+½)].$$

[30] Approximating all components of $\boldsymbol{E}$ at time step $n+½$ by the average of their values at time steps n and $n+1$ and then keeping components of $\boldsymbol{E}^{n+1}(I+1, J+1)$ in the left-hand sides of equations, we obtain the following system of equations:

$$\begin{bmatrix} 1 & 0 & MC_{ey} \\ 0 & 1 & -MC_{ex} \\ -MC_{ey} & MC_{ex} & 1 \end{bmatrix} \begin{bmatrix} E_x^{n+1}(I+1,J+1) \\ E_y^{n+1}(I+1,J+1) \\ E_z^{n+1}(I+1,J+1) \end{bmatrix} = \begin{bmatrix} U_1^{n+1} \\ U_2^{n+1} \\ U_3^{n+1} \end{bmatrix}, \quad (15)$$

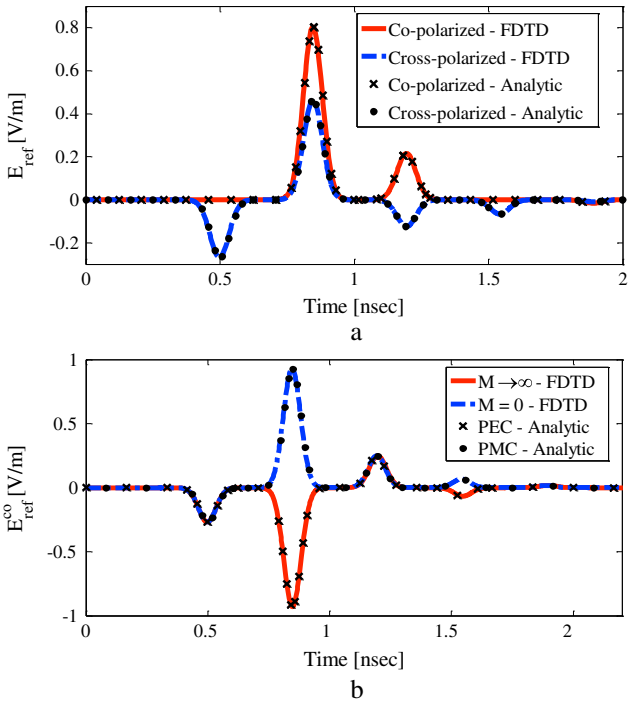

Figure 5. Simulation results of normal incidence of a Gaussian plane wave on a PEMC-backed dielectric slab. (a) Copolarized and cross-polarized reflected fields for the case of $M = 1/\eta_0$. (b) Copolarized reflected field for the cases of $M \to \pm\infty$ (PEC) and $M = 0$ (PMC).

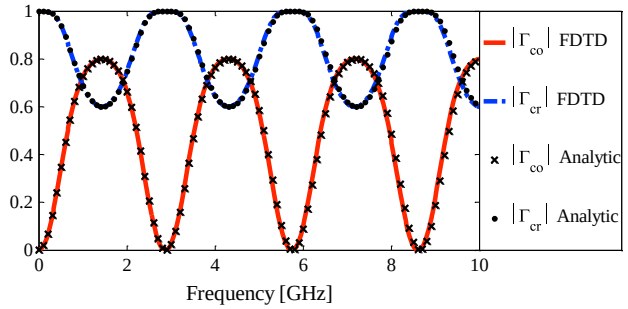

Figure 6. Copolarization and cross-polarization of the reflection coefficient for the case of $M = 1/\eta_0$ in the frequency domain.

where

$$U_1^{n+1} = E_x^n(I+1,J+1) - C_{ey}M\left[E_z^n(I+1,J+1) - E_z^n(I+1,J+½) - E_z^{n+1}(I+1,J+½)\right], \quad (16a)$$

$$U_2^{n+1} = E_y^n(I+1,J+1) + C_{ex}M\left[E_z^n(I+1,J+1) - E_z^n(I+½,J+1) - E_z^{n+1}(I+½,J+1)\right], \quad (16b)$$

$$U_3^{n+1} = E_z^n(I+1,J+1) - C_{ex}[ME_y^n(I+1,J+1) + 2H_y^{n+½}(I+½,J+1)] + C_{ey}[ME_x^n(I+1,J+1) + 2H_x^{n+½}(I+1,J+½)]. \quad (16c)$$

[31] Now the components of $\boldsymbol{E}$ are updated by solving the system of equations (15) as

$$E_x^{n+1}(I+1,J+1) = \frac{1}{1+M^2\left(C_{ex}^2+C_{ey}^2\right)}\left[\left(1+M^2C_{ex}^2\right)U_1^{n+1} + M^2C_{ex}C_{ey}U_2^{n+1} - MC_{ey}U_3^{n+1}\right], \quad (17a)$$

$$E_y^{n+1}(I+1,J+1) = \frac{1}{1+M^2\left(C_{ex}^2+C_{ey}^2\right)}\left[M^2C_{ex}C_{ey}U_1^{n+1} + \left(1+M^2C_{ey}^2\right)U_2^{n+1} + MC_{ex}U_3^{n+1}\right], \quad (17b)$$

$$E_z^{n+1}(I+1,J+1) = \frac{1}{1+M^2\left(C_{ex}^2+C_{ey}^2\right)}\left[MC_{ey}U_1^{n+1} - MC_{ex}U_2^{n+1} + U_3^{n+1}\right]. \quad (17c)$$

[32] From equations (16a), (16b), (17a), and (17b), it is clear that updating components of $\boldsymbol{E}^{n+1}(I+1, J+1)$ requires the z components of $\boldsymbol{E}^{n+1}(I+½, J+1)$ and $\boldsymbol{E}^{n+1}(I+1, J+½)$. Thus, the electric field at the corner needs to be updated after updating that at the boundaries at each integer time step. Finally, the x and y components of $\boldsymbol{H}$ are updated by, first, applying the PEMC boundary conditions $H_{x,y}{}^n(I+1, J+1) = -ME_{x,y}{}^n(I+1, J+1)$ and, next, by approximating $H_{x,y}{}^n \approx ½(H_{x,y}{}^{n+½} + H_{x,y}{}^{n-½})$. Thus. the equation is given by

$$H_{x,y}^{n+½}(I+1,J+1) = -H_{x,y}^{n-½}(I+1,J+1) - ME_{x,y}^n(I+1,J+1). \quad (18)$$

[33] Here we notice that in equation (18), E_x and E_y at $(I+1, J+1)$ are present; hence, these intermediate components need to be updated using equations (17a) and (17b) and stored. At this point, the fields updating equations at the PEMC corner are successfully achieved by equations (17a), (17b), (17c), and (18).

[34] Second, let us consider a PEMC wedge illustrated in Figure 4b. Similar to the corner case, the z component of $\boldsymbol{E}$ and the x and y components of $\boldsymbol{H}$ at the wedge node (I, J) are required for updating fields at adjacent nodes. Hence, they are included in the modified 2-D mesh shown in Figure 4b. Unlike the corner case, the updating equations for the field components at the wedge grid (I, J) are simply achieved by ordinary discretization of Maxwell's curl equations for $\boldsymbol{E}$ and $\boldsymbol{H}$ as follows:

$$E_z^{n+1}(I,J) = E_z^n(I,J) + C_{ex}\left[H_y^{n+½}(I+½,J) - H_y^{n+½}(I-½,J)\right] - C_{ey}\left[H_x^{n+½}(I,J+½) - H_x^{n+½}(I,J-½)\right], \quad (19a)$$

$$H_x^{n+½}(I,J) = H_x^{n-½}(I,J) - C_{hy}\left\{\frac{1}{2}\left[E_z^n(I,J+1) + E_z^n(I,J)\right] - E_z^n(I,J-½)\right\}, \quad (19b)$$

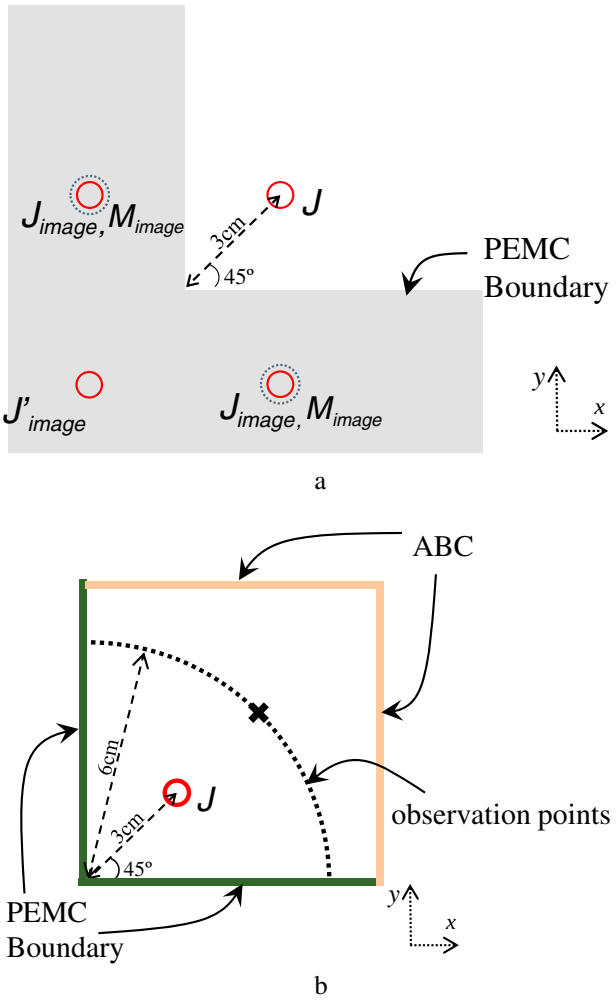

Figure 7. Electric line source scattering by a PEMC 90° corner. (a) Image electric and magnetic currents are displayed; the electric and magnetic currents are shown by solid red and dashed blue circles, respectively. (b) The computational domain used in the FDTD simulation.

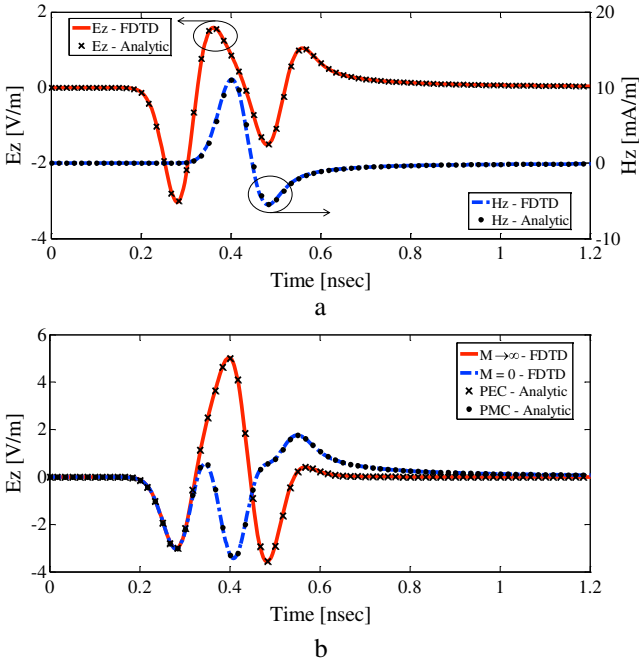

Figure 8. (a) E_z (TM_z) and H_z (TE_z) field components due to scattering by a PEMC corner with $M=1/\eta_0$. (b) E_z (TE_z) field component due to scattering by a PEMC corner with $M\rightarrow\pm\infty$ (PEC) and $M=0$ (PMC).

$$H_y^{n+½}(I,J) = H_y^{n-½}(I,J) + C_{hx} \left\{ E_z^n(I+½,J) - \frac{1}{2}\left[E_z^n(I,J) + E_z^n(I-1,J)\right] \right\}, \quad (19c)$$

where $C_{hx}=\Delta t/\mu_0\delta_x$ and $C_{hy}=\Delta t/\mu_0\delta_y$. In equations (19b) and (19c), the z components of $\boldsymbol{E}$ at $(I, J+½)$ and $(I-½, J)$ are approximated by

$$E_z^n(I,J+½) \approx \frac{1}{2}\left[E_z^n(I,J+1) + E_z^n(I,J)\right],$$

$$E_z^n(I-½,J) \approx \frac{1}{2}\left[E_z^n(I,J) + E_z^n(I-1,J)\right].$$

[35] Deriving field updating equations at the PEMC planar interface, corner, and wedge, one may easily apply the FDTD method on any problem involving PEMC objects.

3. Numerical Results and Validation

[36] The presented algorithm is applied for three different examples. To validate the method, (1) in all examples, results of the proposed algorithm for special cases of the PEMC boundary, i.e., $M\rightarrow\pm\infty$ (PEC) and $M=0$ (PMC), are compared with those of either analytic or conventional FDTD; and (2) in the first two examples, results of the proposed method for an arbitrary value of M are compared with those of existing analytic approaches.

[37] As a first example, normal incidence on a dielectric slab backed by a PEMC is considered. The slab thickness and relative permittivity are assumed to be 5 cm (in the z direction, in accordance to Figure 2) and 3, respectively. The 1-D FDTD computational space is 10 cm, consisting of 200 cells (i.e., $\delta=0.5$ mm), where the slab is assumed to be located between cells 100 and 200 in the right side of the computational space. The soft lattice truncation condition [*Taflove and Brodwin*, 1975] and the PEMC boundary condition, are applied on the left and right sides of the computational space, respectively. To ensure the stability of the algorithm, the Courant stability condition is satisfied by setting the time step $\Delta t=\delta/c_0$, where c_0 is the light

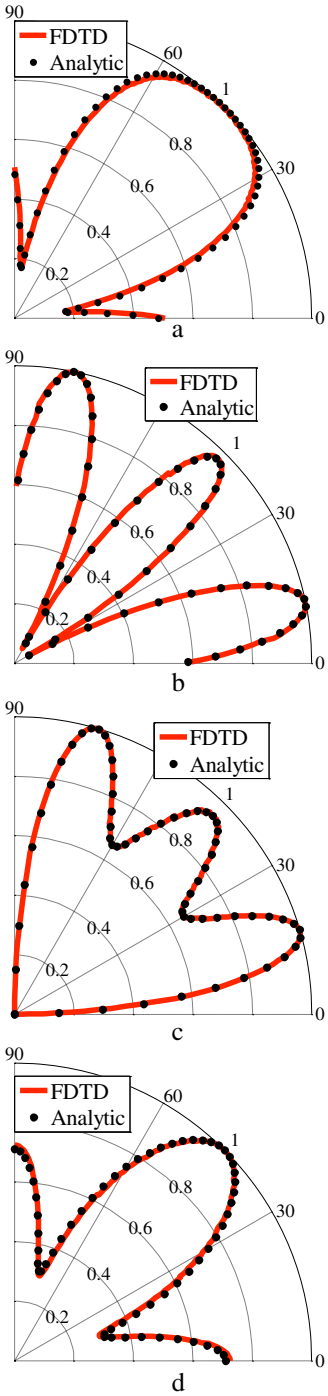

Figure 9. Normalized patterns of (a) E_z and (b) H_z due to scattering by a PEMC corner with $M=1/\eta_0$. Normalized pattern of E_z due to scattering by a PEMC corner with (c) $M\rightarrow\pm\infty$ and (d) $M=0$.

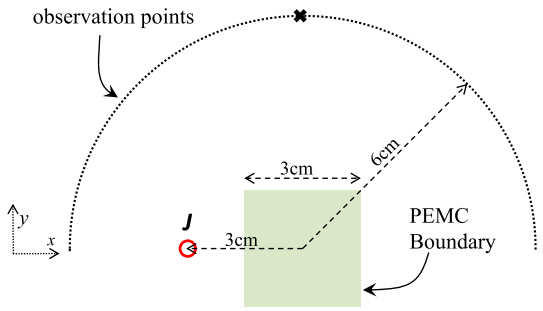

Figure 10. Electric line source scattering by a PEMC square cylinder.

velocity in free space. In FDTD simulations, the slab is illuminated by a x-polarized Gaussian waveform plane wave having a magnitude of unity [i.e., $E_x^{inc}(t)=\exp(-(t-t_0)^2/\beta^2)$ V/m, where $t_0=0.2$ ns and $\beta=0.05$ ns] propagating along the z direction. Co-component and Cross-component of the reflected field, i.e., $E_x^{ref}(t)$ and $E_y^{ref}(t)$, are shown in Figure 5a for the case of the admittance $M=1/\eta_0$. Clearly, for special cases of $M\rightarrow\pm\infty$ (PEC) and $M=0$ (PMC) shown in Figure 5b, the reflected field is copolarized. In addition, the time domain results are transformed into the frequency domain using the discrete Fourier transform (DFT), and co-component and cross-component of reflection coefficient, respectively, defined by $\Gamma_{co}=E_x^{ref}(f)/E_x^{inc}(f)$ and $\Gamma_{cr}=E_y^{ref}(f)/E_x^{inc}(f)$, are calculated. $|\Gamma_{co}|$ and $|\Gamma_{cr}|$ for the case of $M=1/\eta_0$ are shown in Figure 6. Results are compared with those of the analytic technique, based on the method of propagators [*Nayyeri et al*., 2012a], showing accuracy of the presented method.

[38] As a second example, we consider the 2-D test case shown in Figure 7a, which is an electric line source scattering by a PEMC 90° inside corner. As shown in Figure 7a, the line source is along the z axis at the bisector of the corner at a radius of 3 cm. An exact solution of the problem is available using the image theory for PEMC boundaries [*Komijani and Rashed-Mohassel*, 2009b]. According to that theory, to satisfy the boundary condition (1), images of an electric or a magnetic current source above a PEMC boundary are both electric and magnetic currents. The image currents of the electric line source J shown in Figure 7a are given by $J_{image}=J(1-M^2\eta_0^2)/(1+M^2\eta_0^2)$, $M_{image}=-2JM^2\eta_0^2/(1+M^2\eta_0^2)$, and $J_{image}=J$. Here it is noted that M is used as the PEMC admittance and that M_{image} is the image magnetic current. Clearly, for special cases where $M\rightarrow\pm\infty$ (PEC) and $M=0$ (PMC), the magnetic image currents (M_{image}) are omitted, and only the electric image currents remain.

[39] This problem is solved by the proposed 2-D FDTD algorithm in three cases where the PEMC admittance is $M=1/\eta_0$, $M\rightarrow\pm\infty$ (PEC), and $M=0$ (PMC). In our simulations, the size of each 2-D cell is 0.5 mm × 0.5 mm. In order to satisfy the Courant stability criterion, the time step is $\Delta t=0.5\text{ mm}/(\sqrt{2}\,c_0)$. The line source is excited by a Gaussian waveform pulse with a 1 mA magnitude [i.e., $J=\exp(-(t-t_0)^2/\beta^2)$ mA, where the values of t_0 and β are the same as those in the previous example]. Figure 7b shows the computational domain consisting of 150 × 150 cells,

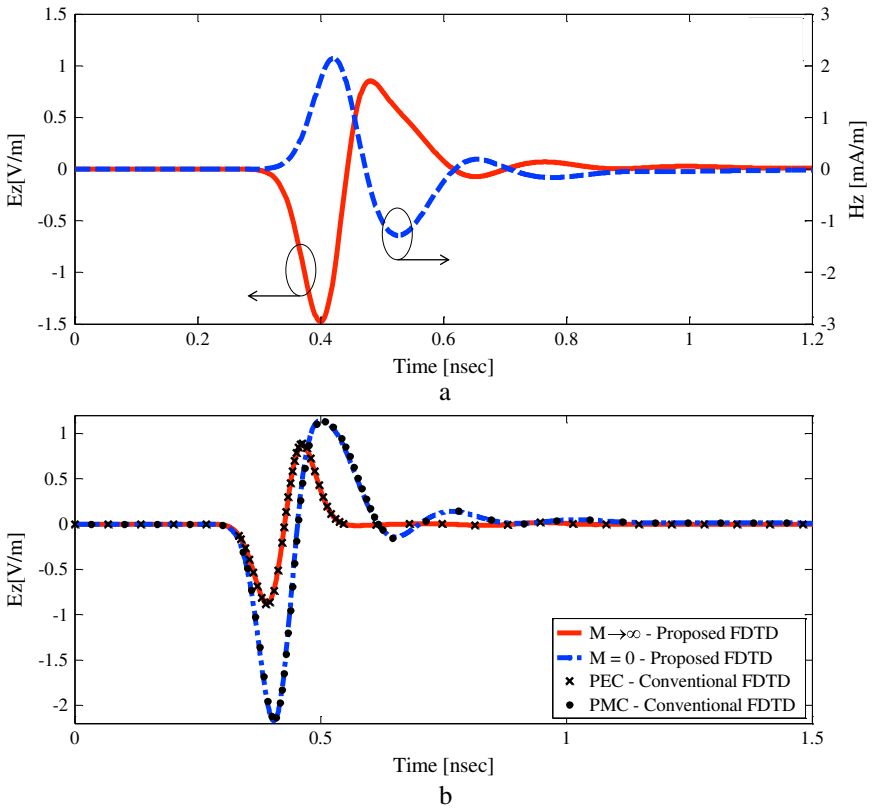

Figure 11. (a) E_z (TM_z) and H_z (TE_z) field components due to scattering by a PEMC cylinder with $M=1/\eta_0$. (b) E_z (TM_z) field component due to scattering by a PEMC cylinder with $M\rightarrow\pm\infty$ (PEC) and $M=0$ (PMC).

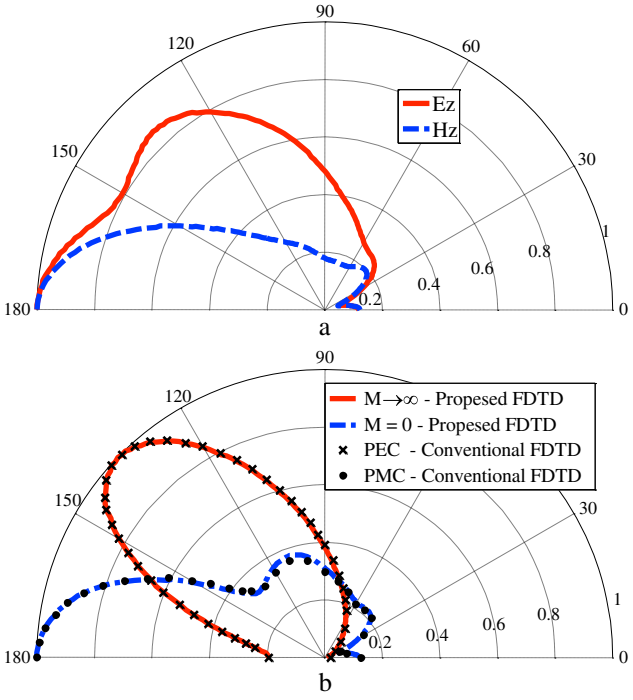

Figure 12. (a) Normalized E_z and H_z patterns due to scattering by a PEMC cylinder with $M = 1/\eta_0$ and (b) that of E_z due to scattering by a PEMC cylinder for two special cases, where $M \to \pm\infty$ (PEC) and $M = 0$ (PMC).

truncated by the PEMC and the absorbing boundary condition (ABC) [*Taflove and Hagness*, 2005]. The values of E_z and H_z corresponding to TE_z and TM_z modes, at 91 points on quarter of a circle (0° to 90°) with a radius of 6 cm (displayed in Figure 7b by a dotted curve), are stored for all time steps. The recorded values of E_z and H_z at a point on the bisector of the corner (the crossed point depicted in Figure 7b) are shown in Figure 8a for the case where $M = 1/\eta_0$ and in Figure 8b for the cases where $M \to \pm\infty$ and $M = 0$. Obviously, for the latter case, TE_z field components are not generated, and only TM_z mode exists. Subsequently, the DFT is used to obtain frequency domain field components' patterns. For the case where $M = 1/\eta_0$, the normalized patterns of E_z and H_z [i.e., $|E_z|/|E_{z,\max}|$ and $|H_z|/|H_{z,\max}|$] at a frequency of 10 GHz are shown in Figures 9a and 9b, respectively. In addition, Figures 9c and 9d, respectively, show the normalized pattern of E_z for the PEC and PMC cases for which $M \to \pm\infty$ and $M = 0$. In both Figures 6 and 7, results of the analytic technique, based on the image theorem, are included for comparison. As shown, excellent agreements emphasize the validity of the presented 2-D algorithm.

[40] Finally, as a third example, to demonstrate the applicability of the presented method to more complex structures, we consider an electric line source scattering by a PEMC square cylinder, as shown in Figure 10. Here the line source is along the z axis at $x = -3$ cm, and a PEMC cylinder with a 3 cm × 3 cm cross section is placed at the coordinate center along the z axis. This problem is also solved by applying the proposed 2-D FDTD algorithm. In our simulation, the computational space is 10 cm × 10 cm, consisting of 200 × 200 cells with a size of 0.5 mm × 0.5 mm. The computational space is truncated by the perfectly matched layer of *Berenger* [1994] with a thickness of 10 cells. Like the previous example, the line source is excited by a Gaussian waveform pulse (with the same parameters), and $\Delta t = 0.5$ mm/($\sqrt{2}c_0$). Values of E_z (TM_z mode) and H_z (TE_z mode), at 181 points on half of a circle (0° to 180°) with a radius of 6 cm (displayed in Figure 10 by a dotted curve), are saved during all time steps and transformed into the frequency domain using the DFT. Figure 11a shows time domain responses of E_z and H_z, for the case where $M = 1/\eta_0$ at the crossed sample point, depicted in Figure 10 (a point on the y axis), and Figure 11b shows that of E_z for the cases of $M \to \pm\infty$ (PEC) and $M = 0$ (PMC). Obviously, for the last two cases, the cross-polarized field (H_z) is not generated since a PEC/PMC cylinder does not generate a cross-polarized wave. Finally, the normalized E_z and H_z patterns for the case where $M = 1/\eta_0$ and that of E_z for both cases $M \to \pm\infty$ and $M = 0$ at a frequency of 10 GHz are shown in Figures 12a and 12b, respectively. Since the solution of this PEMC problem has not yet been reported elsewhere, for special PEC and PMC cases, results validation is carried out through comparisons with those computed using the conventional FDTD method in which, respectively, very large electric and magnetic conductivity is assumed for the cylinder. Comparisons shown in Figures 11(b) and 12(b) demonstrate excellent agreement.

4. Conclusion

[41] In this paper, implementation of the PEMC boundary condition in the FDTD technique is presented. The fact that same components of both ***E*** and ***H*** need to be colocated at both time and space makes this a challenging problem. Hence, first, a modified FDTD mesh is proposed, and then, by properly discretizing Maxwell's curl equations and applying the PEMC boundary condition, appropriate systems of equations for updating fields at the PEMC boundary are obtained. Three different numerical examples are provided to demonstrate the stability and validity of the presented method: reflection from a PEMC-backed dielectric slab and line source scattering from a PEMC 90° corner and a PEMC square cylinder. Validations are made by comparison of the results with those of either existing analytic or conventional FDTD methods applied for some special cases. Although the presented method is to treat 1-D and 2-D problems, it can be extended to 3-D ones as well.

References

Beggs, J. H., R. J. Luebbers, K. S. Yee, and K. S. Kunz (1992), Finite-difference time-domain implementation of surface impedance boundary conditions, *IEEE Trans. Antennas Propag.*, *40*(1), 49–56.

Berenger, J. P. (1994), A perfectly matched layer for the absorption of electromagnetic waves, *J. Comput. Phys.*, *114*(2), 185–200.

Elsherbeni, A., and V. Demir (2009), *The Finite Difference Time Domain Method for Electromagnetics: With MATLAB Simulations*, SciTech, Raleigh, N. C.

Komijani, J., and J. Rashed-Mohassel (2009a), Symmetrical properties of dyadic Green's functions for mixed boundary conditions and integral representations of the electric fields for problems involving a PEMC, *IEEE Trans. Antennas Propag.*, *57*, 3199–3204.

Komijani, J., and J. Rashed-Mohassel (2009b), Green's function for a horizontal source on a dielectric slab with a PEMC ground, paper presented at European Conference on Antennas and Propagation, IEEE, Berlin, Germany.

Kunz, K. S., and R. J. Luebbers (1993), *The Finite-Difference Time-Domain Method for Electromagnetics*, CRC Press, Boca Raton, Fla.

Lindell, I. V., and A. H. Sihvola (2005a), Perfect electromagnetic conductor, *J. Electromagn. Waves Appl.*, *19*(7), 861–869.

Lindell, I. V., and A. H. Sihvola (2005b), Transformation method for problems involving perfect electromagnetic conductor (PEMC) structures, *IEEE Trans. Antennas Propag.*, *53*(9), 3005–3011.

Lindell, I. V., and A. H. Sihvola (2005c), Realization of the PEMC boundary, *IEEE Trans. Antennas Propag.*, *53*(9), 3012–3018.

Lindell, I. V., and A. H. Sihvola (2006a), Losses in the PEMC boundary, *IEEE Trans. Antennas Propag.*, *54*(9), 2553–2558.

Lindell, I. V., and A. H. Sihvola (2006b), The PEMC resonator, *J. Electromagn. Waves Appl.*, *20*(7), 849–859.

Lindell, I. V., and A. H. Sihvola (2006c), Realization of impedance boundary, *IEEE Trans. Antennas Propag.*, *54*(12), 3669–3676.

Lindell, I. V., and A. H. Sihvola (2009), Electromagnetic boundary and its realization with anisotropic metamaterial, *Phys. Rev. E.*, *79*(2), 026,604.

Maloney, J. G., and G. S. Smith (1992), The use of surface impedance concepts in the finite-difference time-domain method, *IEEE Trans. Antennas Propag.*, *40*(1), 38–48.

Nayyeri, V., M. Soleimani, M. Dehmollaian, and J. Rashed Mohassel (2011a), FDTD modeling of dispersive bianisotropic media using *Z*-transform method, *IEEE Trans. Antennas Propag.*, *59*(6), 2268–2279.

Nayyeri, V., M. Soleimani, and M. Dehmollaian (2011b), Analytical and numerical calculation of reflection from a stratified structure backed by a PEMC, paper presented at Mediterranean Microwave Symposium (MMS), IEEE, Hammamet, Tunisia.

Nayyeri, V., M. Soleimani, M. Dehmollaian, and J. Rashed Mohassel (2012a), Reflection from stratified media backed by a perfect electromagnetic conductor (PEMC), *IEEE Trans. Antennas Propag.*, *60*(10), 4969–4973.

Nayyeri, V., M. Soleimani, and M. Dehmollaian (2012b), PEMC-backed perfectly matched layer as a truncation boundary, paper presented at International Symposium on Antennas and Propagation, IEEE, Chicago, Ill.

Nayyeri, V., M. Soleimani, and M. Dehmollaian (2012c), Implementation of a PEMC boundary condition in the 2-D FDTD technique, paper presented at International Symposium on Antennas and Propagation, IEEE, Chicago, Ill.

Nayyeri, V., M. Soleimani, and O. M. Ramahi (2013), Modeling graphene in the finite-difference time-domain method using a surface boundary condition, *IEEE Trans. Antennas Propag.*, *61*(8), pp. 4176–4182, doi:10.1109/TAP.2013.2260517.

Rasouli Disfani, M., K. Vafi, and M. S. Abrishamian (2011), Dyadic Green's function of a PEMC cylinder, *Appl. Phys. A*, *103*(3), 765–769.

Ruppin, R. (2006), Scattering of electromagnetic radiation by a perfect electromagnetic conductor sphere, *J. Electromagn. Waves Appl.*, *20*(12), 1569–1576.

Schuster, J. W., and R. J. Luebbers (1996), Finite difference time domain analysis of arbitrarily biased magnetized ferrites, *Radio Sci.*, *31*(4), 923–929.

Shahvarpour, A., T. Kodera, A. Parsa, and C. Caloz (2010), Arbitrary electromagnetic conductor boundaries using Faraday rotation in a grounded ferrite slab, *IEEE Trans. Microwave Theory Tech.*, *58*(11), 2781–2793.

Sihvola, A. H., and I. V. Lindell (2006), Possible applications of perfect electromagnetic conductor (PEMC) media, paper presented at European Conference on Antennas and Propagation, IEEE, Nice, France.

Sihvola, A. H., P. Yla-Oijala, and I. V. Lindell (2007), Scattering by PEMC spheres using surface integral equation approach, *Appl. Comput. Electromagn. Soc. J.*, *22*(2), 236–249.

Sullivan, D. M. (2000), *Electromagnetic Simulation Using the FDTD Method*, Wiley-IEEE Press, New York.

Taflove, A., and M. E. Brodwin (1975), Numerical solution of steady-state electromagnetic scattering problems using the time-dependent Maxwell's equations, *IEEE Trans. Microwave Theory Tech.*, *23*(8), 623–630.

Taflove, A., and S. C. Hagness (2005), *Computational Electrodynamics: The Finite-Difference Time-Domain Method*, 3rd ed., Artech House, Boston, Mass.

Teixeira, F. L. (2008), Time-domain finite-difference and finite-element methods for Maxwell equations in complex media, *IEEE Trans. Antennas Propag.*, *56*(8), 2150–2166.

Wallen, H., I. V. Lindell, and A. H. Sihvola (2011), Mixed-impedance boundary conditions, *IEEE Trans. Antennas Propag.*, *59*(5), 1580–1586.

Yee, K. S. (1966), Numerical solution of initial boundary value problems involving Maxwell's equations in isotropic media, *IEEE Trans. Antennas Propag.*, *14*(3), 302–307.

Young, J. L. (1994), A full finite difference time domain implementation for radio wave propagation in a plasma, *Radio Sci.*, *29*(6), 1513–1522.